

## Hunting Dark Matter Lines in the Infrared Background with the James Webb Space Telescope

Ryan Janish<sup>\*</sup>

*Fermi National Accelerator Laboratory, Theoretical Astrophysics Department, Batavia, Illinois 60510, USA*

Elena Pinetti<sup>†</sup>

*Fermi National Accelerator Laboratory, Theoretical Astrophysics Department, Batavia, Illinois 60510, USA  
and University of Chicago, Kavli Institute for Cosmological Physics, Chicago, Illinois 60637, USA*

 (Received 17 January 2024; revised 8 October 2024; accepted 18 November 2024; published 18 February 2025)

Dark matter particles with a mass around 1 eV can decay into near-infrared photons. Utilizing available public blank sky observations from the NIRSpec IFU on the James Webb Space Telescope (JWST), we search for a narrow emission line due to decaying dark matter and derive leading constraints in the mass range 0.8–3 eV on the decay rate to photons, and more specifically, on the axion-photon coupling for the case of axionlike particles. We exclude  $\tau < 3.5 \times 10^{26}$  s at  $m_{\text{DM}} \simeq 0.8$  eV and, in the case of axions,  $g_{a\gamma\gamma} > 1.3 \times 10^{-11}$  GeV<sup>-1</sup> for  $m_a \simeq 2.2$  eV. Our results do not rely on dedicated observations, rather we use blank sky observations intended for sky subtraction, and thus our reach may be automatically strengthened as JWST continues to observe.

DOI: [10.1103/PhysRevLett.134.071002](https://doi.org/10.1103/PhysRevLett.134.071002)

**Introduction**—Revealing the nature of dark matter (DM) is one of the most important goals of modern physics. Despite the overwhelming cosmological and astrophysical evidence of its existence, the microscopic properties of DM remain an enigma (see, e.g., [1] for a review). One enticing possibility is that DM is unstable and decays to standard model (SM) states on a cosmological timescale. Astronomical telescopes are ideal instruments to look for a signal from decaying DM in its cosmological environment, where we expect DM to be particularly abundant.

DM candidates decaying into two particles including a photon are of particular interest as they produce a nearly monochromatic emission line which can stand out from the astrophysical background. For instance, DM of mass  $m_{\text{DM}}$  may decay to two photons yielding a line of frequency  $\nu = m_{\text{DM}}/4\pi$ . The mass of the DM candidate then determines the wavelength at which we expect to find an emission line. In particular, DM with mass on the order of an electronvolt would produce photons in the infrared and optical bands. In this work, and for the first time, we search for a DM-produced infrared line in the James Webb Space Telescope (JWST) spectroscopic data. Launched in

2021, JWST is one of the most advanced infrared telescopes, sensitive to wavelengths between 0.6 and 28.3  $\mu\text{m}$ , which corresponds to DM masses between 0.1 and 4.1 eV for a two-photon decay signal.

Our DM search is motivated in particular by the possibility of discovering or constraining axionlike particle DM. Among the numerous theories beyond the standard model that predict compelling DM candidates, axions remain one of the most promising possibilities (see [2,3] and the references therein for a detailed review). They are ultralight pseudoscalar particles which can interact with SM particles such as photons through a dimension-5 operator, and indeed generically decay directly to two photons. Axionlike particles (ALPs) represent the primary example of decaying DM considered in this work.

Throughout this work we use natural units, in which  $\hbar = c = 1$ , unless stated otherwise.

**Dark matter signal**—We will search for an infrared emission line produced by DM. We can parametrize the strength of such emission by the total luminosity produced per DM mass, which we call the *emission rate* and denote  $\Gamma_\gamma$ . For decaying DM,  $\Gamma_\gamma$  is simply the decay rate to photons. The resulting differential energy flux of photons observed by a particular instrument is

$$\Phi_{\text{DM}} = \frac{d\phi}{d\nu d\Omega} = \frac{\Gamma_\gamma}{4\pi} \left( \frac{df}{d\nu} * W \right) D, \quad (1)$$

where  $D$  denotes the so-called  $D$  factor, i.e., the integral of the DM mass density  $\rho$  along the line of sight. In this work we consider the decay of DM particles in the Milky Way

<sup>\*</sup>Contact author: rjanish@fnal.gov

<sup>†</sup>Contact author: epinetti@fnal.gov

TABLE I. Filters and gratings used in this work [7].

Filter-Grating	Wavelengths [ $\mu\text{m}$ ]	Resolution [ $\mu\text{m}$ ]
F100LP-G140M	0.97–1.9	$1.4 \times 10^{-3}$
F100LP-G140M	1.7–3.2	$2.3 \times 10^{-3}$

halo, and we assume a standard NFW DM profile [4,5] with  $r_s = 24$  kpc and  $\rho_s = 0.18$  GeV/cm<sup>3</sup> [6]. Since we do not consider lines of sight that pass near the Galactic Center, we are insensitive to the exact behavior of  $\rho$  as  $r \rightarrow 0$ .

The emission spectrum  $df/d\nu$  specifies the fraction of the total luminosity that is emitted within a frequency interval  $d\nu$ . For simplicity we have assumed that  $df/d\nu$  is uniform in space. We consider the case of monochromatic emission in the DM rest frame, so that  $df/dE$  is set only by Doppler broadening. The fractional width of the line is roughly  $10^{-3}$ , given by the velocity dispersion of the Milky Way. This is the case for decay to two photons, which results in a line at frequency  $\nu_0 = m_{\text{DM}}/4\pi$ . The Doppler width is comparable to the fractional resolution of the medium resolution gratings of JWST NIRSpec used in this work, which have  $\Delta\lambda/\lambda \approx 10^{-3}$  [7], and so we include the Doppler line shape  $df/dE$  in this analysis. We adopt a uniform, isotropic Maxwellian speed distribution, with dispersion  $\sigma_v = 160$  km/s [8]. This is a good approximation for lines of sight that do not pass near the Galactic Center, as we consider here.

The spectrum  $df/d\nu$  is convolved with the instrumental response function  $W$  to produce the observed spectrum. For the instrumental response we take a Gaussian in wavelength [7,9], where the instrumental dispersion  $\sigma_\lambda$  is related to the FWHM resolution  $\Delta\lambda$  as  $\sigma_\lambda = \Delta\lambda/2\sqrt{2 \ln 2}$ .

*James Webb space telescope observations*—Launched on 25 December 2021, the James Webb space telescope [10] is a high-sensitivity and high-resolution infrared telescope covering wavelengths 0.6–28.3  $\mu\text{m}$ . In this work we focus on a select pair of NIRSpec IFU observations [9,11,12], and leave the incorporation of all available and suitable JWST data for future work.

We obtained public data from DDT Program 4426 in Cycle 1, previously used in [13–15]. These are observations from 22–23 May 2023 of the galaxy GN-z11, from which we use only the sky frames. They use two filter or grating combinations, given in Table I. These observations are a good starting point, with a large integration time, sufficient spectral resolution, and targeting a compact source so that much of the field is blank sky. The target is located at Galactic latitude  $b = 54.8^\circ$  and longitude  $l = 126^\circ$  (Note that the absorption in this location is negligible [16,17].), so the line of sight is away from the Galactic Center with  $D \approx 3.8$  GeV kpc/cm<sup>3</sup>  $\approx 1.0 \times 10^7 M_\odot/\text{kpc}^2$ . We use the F100LP-G140M spectrum between 0.99–1.66  $\mu\text{m}$  and F170LP-G235M between 1.66–3.2  $\mu\text{m}$ , which have integration times of 1167 and 1897 s, respectively. The resulting sky spectrum is shown in Fig. 1 and is as expected from studies of the JWST background [18–20].

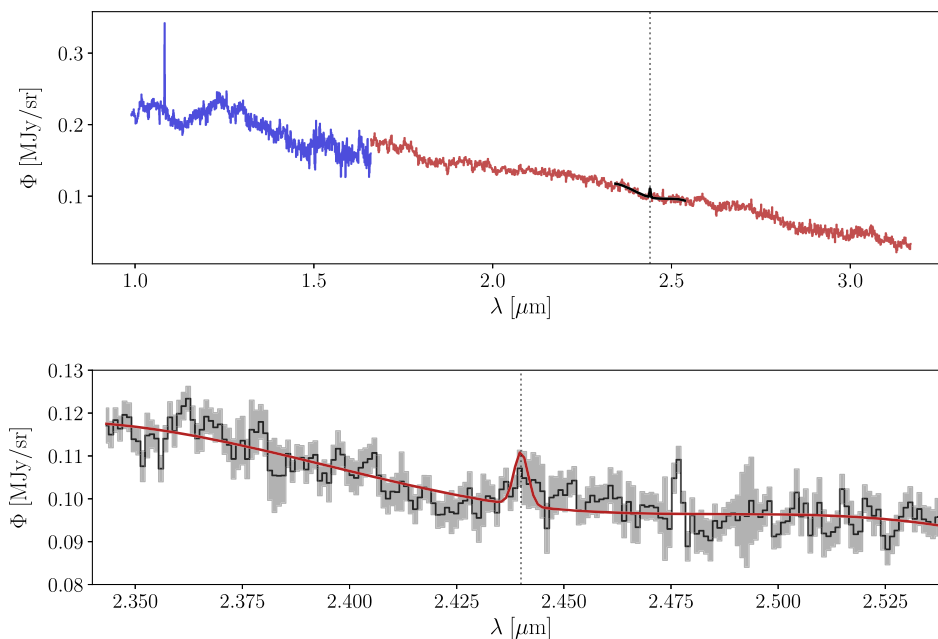


FIG. 1. Top: The spectrum used in this work, with filter-grating F100LP-G140M in blue and F170LP-G235M in red. See text for details. The solid black line illustrates an example continuum fit and DM line at  $\lambda = 2.44$   $\mu\text{m}$ , also indicated by the dotted vertical line. The width of the black line extends over the continuum modeling subregion. See text for details. Bottom: An enlargement of the same spectrum and example DM line, now with the observed spectrum in black, its errors in gray, and the continuum + DM model in red. This DM example corresponds to an ALP of  $m_a = 1.016$  eV and  $g_{\gamma\gamma} = 3.5 \times 10^{-11}$  GeV<sup>-1</sup>, which is allowed at  $2\sigma$ .

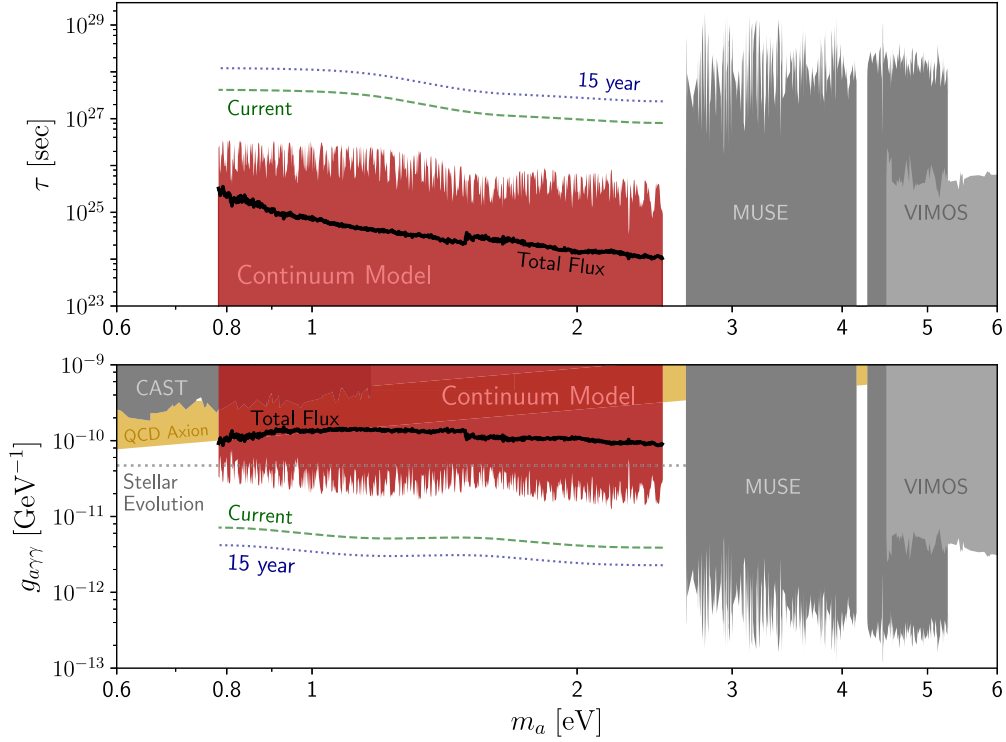


FIG. 2. Top: our results, shown as  $2\sigma$  power-constrained limits on  $\tau = 1/\Gamma_\gamma$  as a function of the DM mass  $m_{\text{DM}}$ , where  $\Gamma_\gamma$  is the DM line luminosity per mass and  $\tau$  is equivalent to the DM to two photon decay rate. Bottom: our  $2\sigma$  power-constrained limits on the ALP-photon coupling  $g_{a\gamma\gamma}$  as a function of ALP mass  $m_a$ , assuming a single ALP species comprises all of galactic DM. Constraints from the total flux are shown in black and constraints using a smooth continuum model in red. Models corresponding to the QCD axion are indicated by the yellow band. The estimated reach after including all JWST data currently observed with NIRSpec using the filters and gratings considered in this work is shown as a green dashed line, as well as after fifteen years of operating time as a blue dotted line. See text for details. The shaded gray regions are already constrained by indirect searches for DM decay [23–26]. The region above the dotted gray line is disfavored by considering the effect of ALP emission on stellar evolution [27,28], however, there is considerable complexity in setting such bounds [29].

*Analysis and results*—We derive two distinct bounds on the DM line emission, and thus on the DM decay lifetime and  $g_{a\gamma\gamma}$  in the case of ALPs. The first we call the *total flux* limit, which roughly requires that the DM flux of Eq. (1) does not exceed the observed flux. This does not rely on a background model and is in that sense conservative. For this bound we use the statistic of [6,21,22]

$$\chi^2_{>} = \sum_i \left( \frac{\max[\Phi_{\text{DM},i}(\Gamma_\gamma, m_{\text{DM}}) - \phi_i, 0]}{\sigma_i} \right)^2, \quad (2)$$

where  $\Phi_{\text{DM},i}$  denotes the predicted flux from DM,  $\phi_i$  is the observed flux and  $\sigma_i$  its uncertainty, and the sum runs over all observed wavelengths. With Gaussian errors and fixed  $m_{\text{DM}}$ , this statistic follows a  $\chi^2$  distribution with one degree of freedom. We scan over  $m_{\text{DM}}$  and set a  $2\sigma$  constraint on  $\Gamma_\gamma$  by requiring  $\chi^2_{>} = 4$ . Our results are shown in Fig. 2.

The second bound constrains the presence of a DM line on top of a generic, smooth continuum, which we call the *continuum model* constraint. This procedure rests on the fact that the JWST background spectrum is dominated by

continuum emission which varies with wavelength only on scales much larger than the DM linewidth [18,19]. This allows the possibility of a DM discovery even without a physical background model, and in the absence of a detection it sets a strong limit by essentially requiring the DM flux to not exceed the size of the fluctuations in the observed spectrum. Thus it is also more constraining when more data is used. Note that we verify the robustness of the continuum background assumption using the JWST background tools [30,31].

We search for a DM line using the test statistic of [6,21,22]

$$\chi^2 = \sum_i \left( \frac{\Phi_{\text{DM},i}(\Gamma_\gamma, m_{\text{DM}}) + P_i(\beta_j) - \phi_i}{\sigma_i} \right)^2. \quad (3)$$

Here the sum runs over an interval of wavelengths centered on the decay wavelength with a width 150 times the FWHM of the DM model line, and  $P$  is a cubic-spline interpolant between five points  $(\lambda_j, \beta_j)$ , where  $\lambda_i$  are fixed wavelengths uniformly dividing the analysis window and

$\beta_j$  are free parameters. This is illustrated in Fig. 1. We estimate the error  $\sigma_i$  by computing a clipped standard deviation of the residuals of a continuum-only fit within each analysis interval, which results in a noise estimate about 2–3 times larger than that provided with the data.

At fixed  $m_{\text{DM}}$  we determine the best-fit  $\hat{\Gamma}_\gamma > 0$  and  $\hat{\beta}_j$  by minimizing  $\chi^2$  and characterize its local  $N\sigma$  significance as

$$\Delta\chi^2 = \chi^2(\hat{\Gamma}_\gamma, \hat{\beta}_j) - \min_{\beta_j} \left[ \chi^2(0, \hat{\beta}_j) \right] = N^2. \quad (4)$$

Scanning over 918 DM mass trials, we find only one line detection with significance exceeding  $5\sigma$ , located at  $1.718 \mu\text{m}$  with local significant  $5.6\sigma$ , as well as the strong, known helium line at  $1.038 \mu\text{m}$  [33,34]. We leave further scrutiny of this line and possible astrophysical backgrounds to future work with more data, and here set upper bounds.

To set upper bounds we use the test statistic of [6,21,22]

$$\Delta\chi^2(\Gamma_\gamma) = \max_{\beta_j} \left[ \chi^2(\Gamma_\gamma, \beta_j) \right] - \chi^2(\hat{\Gamma}_\gamma, \hat{\beta}_j). \quad (5)$$

As argued above for the total flux statistic,  $\Delta\chi^2$  is equivalent to a log-likelihood ratio between the models  $\Phi_{\text{DM}} + P$  with vanishing or positive  $\Gamma_\gamma$ , respectively, with nuisance parameters  $\beta_j$  and assuming the errors are Gaussian distributed. Thus,  $\Delta\chi^2$  follows a  $\chi^2$  distribution with 1 degree of freedom and we set a  $2\sigma$  upper limit by taking  $\Delta\chi^2 = 4$ . Note that these limits are robust to astrophysical emission lines, as the best-fit  $\hat{\Gamma}_\gamma$  will model this line and then  $\Delta\chi^2$  provides a constraint on additional DM emission. We further power constraint our bounds, as in [22] and following the procedure of [35], in order to avoid spurious exclusions due to downward fluctuations in the data. This also makes our limits robust against the presence of background absorption lines.

The analysis presented here employs data with an integration time of roughly 2000 s per data point. The continuum model reach will strengthen as more data is added, and a key virtue of a blank sky search is that a large fraction of all JWST observations will contain blank sky observations. Thus our results may be immediately improved by including all currently available data, and then progressively updated over the lifetime of the instrument. We include in Fig. 2 an estimate of this improved reach, given by scaling the smoothed results of this work to an effective combined integration time according to  $\Gamma_\gamma \propto t_{\text{int}}^{1/2}$  and  $g_{a\gamma\gamma} \propto t_{\text{int}}^{1/4}$ . There is currently  $1.6 \times 10^6$  sec of public data spanning 1.7 calendar years of observing available on MAST from the NIRSpec IFU and MSA, using the high and medium resolution gratings. In Fig. 2 we present an estimate reach for an analysis using all of this data, which we label *current*. Further, we estimate the reach over the lifetime of JWST, which we take to be 15 yr. We take the total future integration time to be 3% of the

mission time, matching the ratio of the first 1.7 yr of available data.

*Conclusions*—In this work, for the first time we constrain the lifetime of decaying DM using measurements from the James Webb space telescope. This work confirms the competitiveness of infrared astronomy to search for and constrain compelling DM candidates. We make use of public blank sky observations, originally collected for the purpose of sky subtraction. In particular, our blank sky approach will allow this DM search to be updated and strengthened as JWST continues to operate, regardless of the specific targets chosen for future observations.

We consider here NIRSpec IFU measurements, which are well suited for blank-sky DM searches. This work focuses on sky spectra collected in tandem with observations of the galaxy GN-z11. We find no significant detection of DM line emission in this data and we considerably improve the bounds on decaying DM in the range 0.8 to 2.5 eV compared to the current bounds in the literature. We exclude a lifetime of  $\tau < 2.6 \times 10^{26}$  s for a DM mass of 1 eV, and up to a maximal constraint of  $\tau < 3.5 \times 10^{26}$  s at  $m_{\text{DM}} = 0.806$  eV. Among the numerous DM candidates in this mass range, axionlike particles (ALPs) are one of the most compelling. For ALP DM, we exclude photon couplings  $g_{a\gamma\gamma} > 2.25 \times 10^{-11} \text{ GeV}^{-1}$  for  $m_a = 1$  eV, down to a maximal constraint of  $g_{a\gamma\gamma} > 1.25 \times 10^{-11} \text{ GeV}^{-1}$  for  $m_a = 2.19$  eV.

We predict that by using all currently collected data we will test lifetimes up to  $3 \times 10^{27}$  s, corresponding to ALP-photon couplings down to  $5 \times 10^{-12} \text{ GeV}^{-1}$ , across the mass window of NIRSpec, 0.5 to 4 eV. We leave this analysis for a future work. With 15 yr of data taking, this may be improved to lifetimes up to  $7 \times 10^{27}$  s and ALP-photon couplings down to  $3 \times 10^{-12} \text{ GeV}^{-1}$ .

*Acknowledgments*—We would like to thank Jorge Martin Camalich, Anirudh Chiti, Shany Danieli, Mike Gladders, Alexander Ji, Kristen McQuinn, Marcia Rieke, Jane Rigby, Jan Scholtz, Jorge Terol Calvo, and Brian Welch for useful conversations, and, in particular, Albert Stebbins for crucial guidance. We express special gratitude to Fengwei Yang and Jeff Dror for a correction on an earlier version of this work. This material is based upon work supported by the U.S. Department of Energy, Office of Science, National Quantum Information Science Research Centers, Superconducting Quantum Materials and Systems Center (SQMS) under Contract No. DE-AC02-07CH11359. We acknowledge support from *Fermi Research Alliance, LLC* under Contract No. DE-AC02-07CH11359 with the U.S. Department of Energy, Office of High Energy Physics.

[1] K. K. Boddy *et al.*, Snowmass2021 theory frontier white paper: Astrophysical and cosmological probes of dark matter, *J. High Energy Astrophys.* **35**, 112 (2022).

- [2] D. J. E. Marsh, Axion cosmology, *Phys. Rep.* **643**, 1 (2016).
- [3] C. B. Adams *et al.*, Axion dark matter, in *Snowmass 2021* (2022), [arXiv:2203.14923](https://arxiv.org/abs/2203.14923).
- [4] J. F. Navarro, C. S. Frenk, and S. D. M. White, The structure of cold dark matter halos, *Astrophys. J.* **462**, 563 (1996).
- [5] M. Cirelli, G. Corcella, A. Hektor, G. Hutsi, M. Kadastik, P. Panci, M. Raidal, F. Sala, and A. Strumia, PPPC 4 DM ID: A poor particle physicist cookbook for dark matter indirect detection, *J. Cosmol. Astropart. Phys.* **03** (2011) 051.
- [6] M. Cirelli, N. Fornengo, B. J. Kavanagh, and E. Pinetti, Integral X-ray constraints on sub-GeV dark matter, *Phys. Rev. D* **103**, 063022 (2021).
- [7] Nirspec dispersers and filters, <https://jwst-docs.stsci.edu/jwst-near-infrared-spectrograph/nirspec-instrumentation/nirspec-dispersers-and-filters> (2017).
- [8] N. W. Evans, C. A. J. O'Hare, and C. McCabe, Refinement of the standard halo model for dark matter searches in light of the Gaia sausage, *Phys. Rev. D* **99**, 023012 (2019).
- [9] P. Jakobsen, P. Ferruit, C. Alves de Oliveira, S. Arribas, G. Bagnasco, R. Barho *et al.*, The near-infrared spectrograph (NIRSpec) on the James Webb Space Telescope. I. Overview of the instrument and its capabilities, *Astron. Astrophys.* **661**, A80 (2022).
- [10] J. P. Gardner *et al.*, The James Webb Space Telescope, *Space Sci. Rev.* **123**, 485 (2006).
- [11] B. J. Rauscher *et al.*, Detectors for the James Webb Space Telescope near-infrared spectrograph. 1. Readout mode, noise model, and calibration considerations, *Publ. Astron. Soc. Pac.* **119**, 768 (2007).
- [12] T. Böker, S. Arribas, N. Lützgendorf, C. Alves de Oliveira, T. L. Beck, S. Birkmann *et al.*, The near-infrared spectrograph (NIRSpec) on the James Webb Space Telescope. III. Integral-field spectroscopy, *Astron. Astrophys.* **661**, A82 (2022).
- [13] R. Maiolino *et al.*, JWST-JADES. Possible Population III signatures at  $z = 10.6$  in the halo of GN-z11, *Astron. Astrophys.* **687**, A67 (2024).
- [14] The data described here may be obtained from <http://dx.doi.org/10.17909/j5c2-c258>.
- [15] J. Scholtz, C. Witten, N. Laporte, H. Ubler, M. Perna, R. Maiolino *et al.*, GN-z11: The environment of an AGN at  $z = 10.603$ , *Astron. Astrophys.* **687**, A283 (2024).
- [16] D. J. Schlegel, D. P. Finkbeiner, and M. Davis, Maps of dust IR emission for use in estimation of reddening and CMBR foregrounds, *Astrophys. J.* **500**, 525 (1998).
- [17] Galactic dust reddening and extinction, <https://irsa.ipac.caltech.edu/applications/DUST/>.
- [18] J. E. Krick, W. J. Glaccum, S. J. Carey, P. J. Lowrance, J. A. Surace, J. G. Ingalls, J. L. Hora, and W. T. Reach, A Spitzer/IRAC measure of the zodiacal light, *Astrophys. J.* **754**, 53 (2012).
- [19] J. R. Rigby, P. A. Lightsey, M. García Marín, C. W. Bowers, E. C. Smith, A. Glasse *et al.*, How dark the sky: The JWST backgrounds, *Publ. Astron. Soc. Pac.* **135**, 048002 (2023).
- [20] JWST background model, <https://jwst-docs.stsci.edu/jwst-general-support/jwst-background-model> (2017) Accessed: 2023-08-07.
- [21] G. Cowan, K. Cranmer, E. Gross, and O. Vitells, Asymptotic formulae for likelihood-based tests of new physics, *Eur. Phys. J. C* **71**, 1554 (2011).
- [22] B. M. Roach, S. Rosslund, K. C. Y. Ng, K. Perez, J. F. Beacom, B. W. Grefenstette, S. Horiuchi, R. Krivonos, and D. R. Wik, Long-exposure NuSTAR constraints on decaying dark matter in the Galactic halo, *Phys. Rev. D* **107**, 023009 (2023).
- [23] E. Todarello, M. Regis, J. Reynoso-Cordova, M. Taoso, D. Vaz, J. Brinchmann, M. Steinmetz, and S. L. Zoutendijk, Robust bounds on ALP dark matter from dwarf spheroidal galaxies in the optical MUSE-Faint survey, *J. Cosmol. Astropart. Phys.* **05** (2024) 043.
- [24] D. Grin, G. Covone, J.-P. Kneib, M. Kamionkowski, A. Blain, and E. Jullo, A telescope search for decaying relic axions, *Phys. Rev. D* **75**, 105018 (2007).
- [25] CAST Collaboration, An improved limit on the axion-photon coupling from the CAST experiment, *J. Cosmol. Astropart. Phys.* **04** (2007) 010.
- [26] CAST Collaboration, New CAST limit on the axion-photon interaction, *Nat. Phys.* **13**, 584 (2017).
- [27] A. Ayala, I. Domínguez, M. Giannotti, A. Mirizzi, and O. Straniero, Revisiting the bound on axion-photon coupling from globular clusters, *Phys. Rev. Lett.* **113**, 191302 (2014).
- [28] M. J. Dolan, F. J. Hiskens, and R. R. Volkas, Advancing globular cluster constraints on the axion-photon coupling, *J. Cosmol. Astropart. Phys.* **10** (2022) 096.
- [29] C. Severino and I. Lopes, Asteroseismology: Looking for axions in the red supergiant star Alpha Ori, *Astrophys. J.* **943**, 95 (2023).
- [30] <https://jwst-docs.stsci.edu/jwst-other-tools/jwst-backgrounds-tool#gsc.tab=0>
- [31] The astrophysical background can be decomposed into four components: interstellar medium emission, zodiacal light, detector stray light, and thermal self-emission. In the wavelength range of interest, the total background is primarily dominated by the continuum emission from zodiacal light [30,32].
- [32] W. T. Reach, P. Morris, F. Boulanger, and K. Okumura, The mid-infrared spectrum of the zodiacal and exozodiacal light, *Icarus* **164**, 384 (2003).
- [33] J. Strader, A. K. Dupree, and G. H. Smith, The 10830 Å helium line among evolved stars in the globular cluster M4, *Astrophys. J.* **808**, 124 (2015).
- [34] A. Oklopčić and C. M. Hirata, A new window into escaping exoplanet atmospheres: 10830 Å line of helium, *Astrophys. J. Lett.* **855**, L11 (2018).
- [35] G. Cowan, K. Cranmer, E. Gross, and O. Vitells, Power-constrained limits, [arXiv:1105.3166](https://arxiv.org/abs/1105.3166).